King Saud University

Arabian Journal of Chemistry

www.ksu.edu.sa
www.sciencedirect.com

ORIGINAL ARTICLE

Antimicrobial and cytotoxicity properties of biosynthesized gold and silver nanoparticles using *D. brittonii* aqueous extract

Palaniselvam Kuppusamy [a], Sujung Kim [b], Sung-Jo Kim [c], Ki-Duk Song [a,b,*]

[a] *The Animal Molecular Genetics and Breeding Center, Jeonbuk National Universibty, Jeonju 54896, Korea*
[b] *Department of Agricultural Convergence Technology, Jeonbuk National University, Jeonju 54896, Korea*
[c] *Division of Cosmetics and Biotechnology, College of Life and Health Sciences, Hoseo University, Baebang, Asan 31499, Korea*

Abstract Recently, the production of nanoparticles using biological resources has gained considerable attention due to their application for animal and human well-being. In this study, we used a green synthesis to fabricate gold and silver nanoparticles by reducing $HAuCl_4$ and $AgNO_3$ into AuNPs and AgNPs, respectively, using *Dudleya brittonii* (DB) extract. The physio-chemical properties of the synthesized nanoparticles were analyzed using a UV–vis spectrophotometer, FESEM, EDX, HR-TEM, AFM and FT-IR. Furthermore, the antimicrobial and cytotoxicity activities of DB-AuNPs and DB-AgNPs against livestock pathogenic bacteria and different cell lines, as well as anti-oxidant activity, were investigated. DB synthesized AuNPs and AgNPs were mostly spherical with a few triangular rods and sizes ranging of 5–25 nm and 10–40 nm, respectively. The in *vitro* antibacterial and antifungal studies demonstrated the DB-AuNPs and DB-AgNPs have good antibacterial activity against *E. coli* and other livestock pathogens, including *Y. pseudotuberculosis* and *S. typhi*. Cell studies revealed that the higher concentrations of both DB-AuNPs and DB-AgNPs (1 μg/ml to 1 mg/ml) showed potent cytotoxicity in chicken cells after 24 hrs, whereas the middle and lower concentrations of DB-AuNPs and DB-AgNPs did not show cytotoxicity in selected cell lines after 24 hrs. In addition, the DB synthesized AuNPs and AgNPs exhibited good free scavenging activity in a dose-dependent manner. Therefore, the biosynthesized nanoparticles can be utilized by the livestock industry to develop an effective source against livestock microbial infections.

* Corresponding author at: Department of Animal Biotechnology & The Animal Molecular Genetics and Breeding Center, Jeonbuk National University, Jeonju 54896, Korea.
E-mail address: kiduk.song@jbnu.ac.kr (K.-D. Song).

Production and hosting by Elsevier

1. Introduction

Nanotechnology is one of the most dynamic fields within science and engineering research. Recently, the production of nanoparticles using a green approach has steadily gained interest among the international community towards improving environmental conditions, sustainable development, and minimizing the effect of harmful man-made wastes for promising applications in human health and agriculture areas (Arvizo et al., 2010; Erdogan et al., 2019; Alabdallah and Hasan, 2021). The green synthesis of nanoparticles potentially offers easy-to-handle, one pot reaction, economic and environmental-friendly advantages in the production of nanoparticles for various applications, including agriculture, adjuvants in vaccine development and biomedical uses (Saif et al., 2016; Rónavári et al., 2021). Till date, a diverse group of plant species, microorganisms and their byproducts were used for the green synthesis of metallic nanoparticles. In particular, the biosynthesis of nanoparticles using plant extracts is more expedient and easier than that using microorganisms. Besides, microbial culture requires a wide range of downstream processes that are more expensive than plant extracts in the synthesis of nanomaterials (Kuppusamy et al., 2016; Lee et al., 2018). Kumar et al. (2011) suggest that biosynthesis approaches have the potential to generate less waste and more productivity in an eco-friendly manner compared to traditional approaches (Kumar et al., 2011). The synthesis of nanoparticles with desired sizes, shapes, and monodispersity nature is highly challenging in terms of unique applications and associated nano-based product development. Conventional fabrication of nanoparticles can be used to synthesize unique sizes and morphologies. On the other hand, these methods are laborious, tedious procedures with hazardous chemical uses that cause the environment to be unsafe and less suitable for biomedical applications (Xin Lee et al., 2016; Murad et al., 2018; Koul et al., 2021). Therefore, it is necessary to develop a sustainable, reliable, and eco-friendly method for the fabrication of metal nanoparticles. This can be achieved by synthesizing of nanoparticles using biological substances such as plant extracts, microorganisms, algae, seaweeds, enzymes, fungi, mushrooms, and biological polymers. Also, the biological synthesis method could control the toxicity and size optimization at pilot scale production of nanoparticles (Nath and Banerjee, 2013; Rauf et al., 2021).

Nanoparticles are commonly categorized into two major classes, i.e., organic and inorganic nanoparticles. Organic nanoparticles encompass metallic (Au, Ag, Cu), magnetic (Co and Ni), and semi-conductors (Zn, $CaSo_4$) types, whereas inorganic nanomaterials include carbon based materials such as carbon nanotubes and quantum dots (Zhang et al., 2016; Bamal et al., 2021; Tehri et al., 2022). Metal based nanoparticles, mainly Au and Ag are extensively used in commercial and biomedical applications due to their unique tuneable electrical, photo-thermal, and biocompatible properties. These nanosized materials can be used in different applications, including biosensor development, diagnostic imaging, therapeutic agents, bio labelling, waste water treatment, catalysis, and delivery of drugs and gene (Watanabe et al., 2006; Zayed et al., 2019; Botteon et al., 2021). The gold nanoparticles (AgNPs) are active against pathogenic microorganisms, different cancer cells, and many other acute diseases. These nanosized materials have a large surface area, that can simultaneously integrate with drugs to target specific sites for treatment and imaging agents, which can be useful for cancer treatments and other clinical applications (Wei et al., 2015; Das et al., 2021). Metallic silver nanoparticles (AgNPs) are extensively used as antimicrobial agents, personal care products, drug carriers in cancer treatments, vaccine adjuvants, anti-aging and anti-inflammatory agents. Plant broth contains a complex variety of nutrients and bioactive metabolites (flavonoids, amino acids, proteins, fatty acids, carbohydrates, phenolic, alcohols, and alkaloids) that play a crucial role in nanoparticle formation, reduction, and capping agents (Mat Yusuf et al., 2020; Mohammadinejad et al., 2019).

Deldleya brittonii (DB) belongs to the succulent plant, and it is widely used as an ornament. DB can be found in a variety of locations, including California and Mexico. The biological activities of the *D. brittonii* is yet elucidated. Interestingly, Mulroy, (1979) discovered that the *D. brittonii* is useful in treating respiratory related diseases such as asthma and inflammatory airway obstruction diseases, which are closely associated with macrophage cells. Recently, we reported that *D. brittonii* succulent plant extract improved respiratory function and immune function in macrophage alveolar cells. DB exposure in macrophage cells reduced PMA-induced cell death and enhanced anti-inflammatory efficacy (Kim et al., 2019). Similarly, *Aloe vera*, belongs to the succulent plant family, contains different bioactive compounds such as proteins, polysaccharides, polyphenols, aldehydes, ketones, hemicellulose, lignin and pectin. These bioactive metabolites effectively act in the reduction of silver ions and produce potent antibacterial AgNPs from *Aloe vera* (Tippayawat et al., 2016). Aqueous extract of *F. retusa* leaves aqueous extract is a simple and inexpensive material to synthesize gold and silver nanoparticles using green route approaches (Zayed et al., 2019). However, succulent plants have not been reported extensively in the literature. Particularly, the DB succulent has attracting wide range of consumers due to their potent physiological properties. And it is also used traditionally to treat various digestive related diseases, anti-inflammatory and skin infections (Hwang, 2021). In addition, DB is commercially well known succulent plant and did not reported their bioactivity yet. Therefore, in this study, we synthesized AuNPs and AgNPs in an environmentally friendly manner using *D. brittonii* aqueous extract and characterized their biological applications against pathogenic bacteria and various cell cultures.

2. Materials and methods

2.1. Chemicals used

Tetra chloroauric acid, silver nitrate, sodium chloride, NaOH and HCl were purchased from Merck, Korea. Cell culture reagents and plastic wares were purchased from Thermo-Fisher Scientific, Korea. Pathogenic bacteria and fungal cultures were obtained from the Department of Biotechnology, Center for Industrialization of Agricultural and Livestock Microorganisms (CIALM), Jellobuk-do, Korea. All reagents used were HPLC grade.

2.2. Plant collection and extract preparation

D. brittonii plants (Fig. 1a) were purchased from a commercial market located in Asan, Korea. The purchased plants were grown at the Department of Biotechnology, Hoseo University, Asan, Korea. 50 g of fresh leaves were cut into small pieces (1–2 cm) and 150 ml of distilled water was added. The mixture was extracted at 110 °C and 39.23 kPa for 10 min using an autoclave machine. The extract was sterile filtered with a 0.22 μm pore size cellulose-acetate filter (Sartorius, Goettingen, Germany) and stored at 4 °C for further experiments use (Kim et al., 2019).

2.3. Synthesis of AuNPs and AgNPs using a bio-fabrication method

One pot synthesis of Au and Ag nanoparticles using *D. brittonii* extract was carried out as follows: Synthesis of AuNPs was performed with $HAuCl_4$ and aqueous *D. brottonii* extract. Briefly, 5 ml of DB plant extract was mixed with 45 ml of
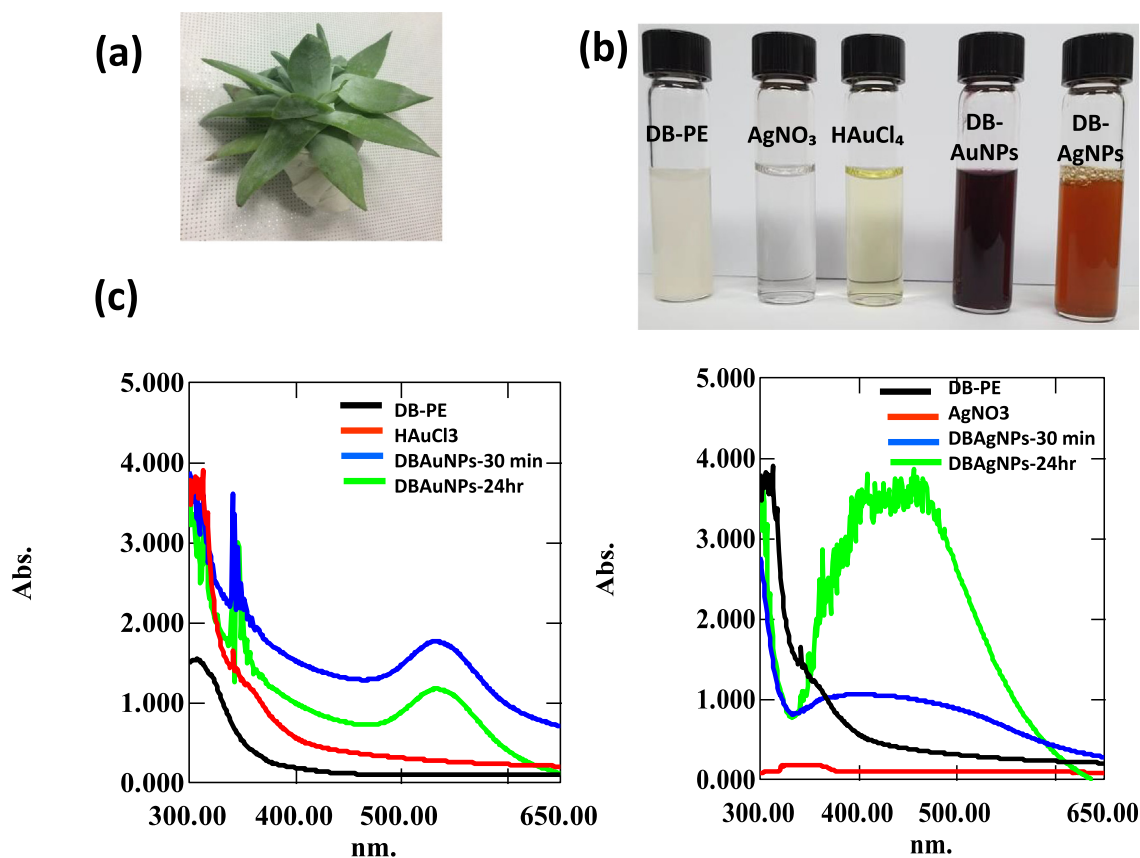
Fig. 1 UV–Visible spectra of DB synthesized AuNPs and AgNPs solution measured at 30 min and 24 hr time intervals. (a) Photograph of *D. brittonii* (b) Color indicates the redox reaction of DB plant extract (DB-PE), HAuCl$_4$, AgNO$_3$, DB-Au, DB-Ag nanoparticle (c) The UV–vis spectra of DB-AuNPs and DB-AgNPs exhibited absorption peaks at 535 and 456 nm, respectively.

aqueous solution of 10^{-3} M HAuCl$_4$. The color of the reaction solution changed immediately in the solution, and then the reaction mixture was kept on a hot plate at 35 °C, and stirred for 30 min to completely reduce metal ions in the solution. This was done to enhance the interaction of non-reduced ions with plant compounds present in the medium. For the synthesis of AgNPs, 5 ml of plant extract was mixed with an AgNO$_3$ (10^{-3} M) solution. The mixture solution appeared as a yellowish-brown color within 15 min, which indicated the silver nanoparticle synthesis process in the mixture (Tamuly et al., 2013). The synthesized nanoparticle solution was centrifuged at 10,000 × g for 15 min, and the resulting pellets were freeze-dried and stored at 4 °C until further use. Also, the synthesized reaction mixture was optimized using three parameters, including pH, extract quality, and metal salt concentration. These parameters influenced the size and structure of AuNPs and AgNPs synthesized using a green synthesis procedure.

2.4. Characterization of synthesized Au and Ag nanoparticles

Ultraviolet–visible (UV–vis) spectra of biosynthesized gold and silver nanoparticles were measured using a UV–vis Spectrophotometer (Shimadzu 1800 model, Japan) at 200–800 nm wavelength scan range, and a resolution of 1 nm. The absorption value obtained for each sample, including nanoparticles and the metal ion solution, was subtracted from their corresponding blank solution.

The size, morphology, purity and elemental composition of the synthesized Au and Ag nanoparticles were observed using Field emission scanning electron microscope (FESEM), Energy dispersive X-ray spectroscopy (EDX), elemental mapping with consisted of FESEM electron microscope (JEOL, JEM2100 F, USA) operated at 200 kV. For FESEM sample preparation, the freeze-dried samples were placed on carbon film in a sample holder and sputter coated at 90 °C for 90 s. The TEM instrument was also used to characterize the sizes, shapes, and particle distribution of AuNPs and AgNPs. The few droplets of purified aqueous nanoparticles samples were placed on carbon-coated copper grids and dried on a hot plate at 80 °C for 10 min, and analyzed using the TEM instrument.

XRD was performed for the analysis of the crystalline phases of the synthesized AuNPs and AgNPs. The powder form of the nanoparticles was studied on X-ray spectrophotometer, (D7 Advance, MA, USA) under the following operating conditions: 40 k voltage, 30 mA, Cu-Ka radiation of 1.5406Å, wavelength at a scanning rate of 1 °C/min, over the scan range from 5 to 90˚ (2θ). Reference XRD patterns of Au and Ag were obtained from the International Center for Diffraction Data (ICDD).

FT-IR spectrophotometer analysis provided the functional groups which involved in the reduction and catalytic agents for the formation of Au and Ag nanoparticles using DB extract. FT-IR measurements were performed using biosynthesized AuNPs and AgNPs powder samples by a FT-IR spectrophotometer using the kBr method (PerekinElmer, USA), with a

scan range of 4000–500 cm^{-1} and a resolution of 1 cm^{-1}. The spectra values are obtained and plotted as transmittance (%) versus wave number (cm^{-1}).

2.5. Biological applications of synthesized AuNPs, AgNPs

2.5.1. Antimicrobial activity of AgNPs and AuNPs

The DB extract and synthesized gold and silver nanoparticles (different dilutions 10^{-1} −10^{-9}; stock concentration was prepared 10 mg/ml) were tested for their antibacterial activity against various livestock pathogens such as, *E. coli* (KCTC2617), *Salmonella derby* (NCCP 12238), *Salmonella enteritidis* (NCCP 14546), *Salmonella typhimurium* (NCCP 10438), *Yersinia enterocolitica* (NCCP 11129), *Yersinia pseudotuberculosis* (NCCP 11125) and *Clostridioides difficile* (JCM 1296) using the agar disc diffusion method. Briefly, the Luria-Bertani (LB) agar, Sabouraud Dextrose (SD) Agar and Brain Heart Infusion Agar plates were used as a bacterial growth medium. 100 µL of each bacterial suspension (1.2 X 10^8 CFU/ml) was spread on a solidified agar plate. The DB-AuNPs, DB-AgNPs, and plant extract were prepared, and each 20 µL sample was impregnated into sterile 6 mm discs. The spotted nanoparticles solution and DB extract on the disc were allowed to dry, and the disc was placed on the bacterial inoculated agar plate. The disc-inoculated agar plates were incubated at 37 °C for 24 hrs in a humidified incubator. The antibiotic ampicillin (1 mg/ml) was used as a positive control and a sterile distilled water disc was used as a negative control. After incubation time, the agar plates were measured for the zone of inhibition around the discs. The assay was repeated in triplicate (Donga et al., 2020).

Antifungal activity was evaluated against *Candida tropicalis* (NCCP 30262), *Candida albicans* (NCCP 31077) and *Candida glabrata* (NCCP 30939) using the agar disc diffusion method. For analysis of the fungicidal effects of biosynthesized DB-AuNPs DB-AgNPs, and DB-extract, we used three *Candida* strains. The fungal cultures were grown on a LB agar medium. 200 µL of the culture (1.2 X 10^8 colonies/mL) were spread immediately. 20 µL of AuNPs, AgNPs and DB extract were separately added to sterile filter paper blank disc and allowed to absorb completely. The dried sample disc were then placed on the fungal inoculated plates. The standard drug gentamycin (1 mg/ml) was used as the positive control for this experiment. The plates were incubated at 25 °C for 48 hrs, and subsequently, the inhibition zone was measured in the experimental agar plate. The assay was conducted in triplicate (Mohanta et al., 2017).

2.5.2. Antioxidant activity of AgNPs and AuNPs

DPPH (2, 2-diphenyl1-picrylhydrazyl) free radical scavenging activity of the AuNPs, AgNPs and DB extract was measured using the protocol reported by Kharat and Mendhulkar (2016) with slight modification. About 0.3 mM of DPPH (9.5 mg) was dissolved in methanol (50 ml) solution. Different concentrations of both Au and Ag nanoparticles (dilution 10^{-1}, 10^{-2}, 10^{-3}, 10^{-4} and 10^{-5}, stock concentration was prepared at 10 mg/ml) were prepared and mixed with 200 µL of DPPH methanolic solution. The control sample contains only methanol and DPPH solution, and ascorbic acid was used as standard (5 mg/ml). The mixture solution was incubated for 30 min at room temperature in a dark condition. Subsequently, the absorbance of the OD value was recorded at 517 nm for samples, standard, and positive control. The DPPH mixture's decreased absorbance values may indicate higher antioxidant activity in the samples. DPPH antioxidant activity was determined by following formula: % DPPH free radical scavenging activity = [(absorbance of control-absorbance of sample)] / [(absorbance of blank-absorbance of control)] × 100.

2.5.3. Cytotoxicity activity of AgNPs and AuNPs against different cell lines

The cytotoxicity of DF-1 cells (chicken embryonic fibroblast cells), HD 11 (chicken macrophage cells) and HT-29 (human colon cancer cells) was evaluated using synthesized AuNPs and AgNPs by WST-1 cell cytotoxicity assay. Chicken fibroblast cells, macrophage cells, and human colon cancer cells were cultured in Dulbecco Modified Eagles Medium (DMEM) with 10 % fetal bovine serum and 1 % penicillin and streptomycin (ATCC, MA, USA) at 37 °C in a humidified condition with 5 % CO$_2$. The cells were seeded in a 96-well plate at a density of 5X10^3 cells per well. After confluence reached to 70–75 %, the medium was replaced with a different concentration of synthesized nanoparticles (DB-AuNPs and DB-AgNPs) and incubated for 24 hrs. The cells without nanoparticles were used as a control. After incubation, a cell viability assay was performed using WST-1 tetrazolium dye (Sigma-Aldrich, Korea) according to the manufacture's guidelines. 10 µL of WST-1 reagent was added to each well and incubated for 3 hrs. Finally, the absorbance of each well was measured using an ELISA reader at 490 nm (Bilgic et al., 2021). Experiments were conducted in triplicate, and the mean and standard error were calculated. The cell viability percentage was assessed by using the following equation: Cell viability (%) = (sample OD-blank OD) / (control OD-blank OD) × 100 %.

2.6. Statistical analysis

All experiments were performed in triplicate. Data were expressed as mean and ± SE. One-way ANOVA was used to compare the difference among samples/groups, followed by Duncan's multiple range test. A P-value of less than 0.05 was considered to be statistically significant, as indicated by different subscript letters (a, b, c and d) in the figures and tables.

3. Results and discussion

3.1. UV–Visible spectrum of synthesized DB-AuNPs and DB-AgNPs

The biosynthesis of metal nanoparticles was preliminarily confirmed by the rate of color appearance in the colloidal mixture solution. In this case, the color of DB synthesized AuNPs changed from colorless, turbid into a pale pink color and AgNPs changed from colorless into a brownish yellow color (Fig. 1b), which were visual indications of metal nanoparticle presence in the sample. Then, the synthesized sample was confirmed by a UV–vis spectrophotometer. The UV–vis spectra analysis revealed that the maximum absorbance peaks were found at 535 nm and 456 nm for gold and silver nanoparticles, respectively. The gold and silver NPs exhibited a single broad,

sharp SPR on the UV–vis spectrum (Fig. 1c), which indicated the attainment of bio-reduction of metal ions. Furthermore, the colloidal nanoparticle solutions were kept for 30 days to evaluate the stability of synthesized nanoparticles. After 30 days, there were no changes observed in color and their absorbance spectrum (not shown).

The optimization of synthesis reaction was evaluated in terms of reproducibility and production efficiency of the biosynthesis method. The size and morphology of nanoparticles are regulated by the optimization of reaction parameters. Thus, the principal parameters, including pH, metal salt concentration, and plant extract ratio, were investigated (Fig. 2a-f). To enhance the yield and efficiency of the production of NPs, the different parameters such as pH (4, 5, 6, 7 and 8), metal salt concentration (10^{-2}, 10^{-3} and 10^{-4}) and plant extract ratios (1:1, 1:2, 1:3) were fixed. We found at room temperature, 5 ml of aqueous DB extract effectively reduced 45 ml of aqueous metal salt solution (10^{-3} M), suggesting that the synthesis of AuNPs and AgNPs appeared faster than other reaction conditions (Fig. 2a-f). The UV–vis spectra analysis also determined the optimal parameters based on the SPR value and absorption bands that could lead to the formation of nanoparticles in the colloidal solution. Many reports have been previously published on the successful synthesis of gold and silver nanoparticles using various plant extracts such as *Euphorbia hirta* (Annamalai et al., 2013), *Torreya nucifera* (Kalpana et al., 2019), *Arachis hypogaea* (Raju et al., 2014), *Rosa indica* (Manikandan et al., 2015), and *Terminalia arjuna* (Suganthy et al., 2018). Among the different parameters, the color change is a preliminary qualitative method of detecting plant extract for biological reduction of metal ions into metal NPs (Wang et al., 2009; Doan et al., 2020). The color specificity of the medium may vary due to the phytochemical content present in the plants. Also, the plant compositions will vary based on region of growth, soil nature, nutritive value, and other environmental factors. These characteristics affect the composition of plant extracts used for reduction reactions (Hussain et al., 2019). Basically, the UV–vis spectra analysis shows the SPR band of Au and Ag nanoparticles at approximately 500–550 nm and 400–450 nm, respectively. We found that the UV–visible spectra absorption bands were at 535 for AuNPs and 410 for AgNPs formation in DB extract. Both bands were observed to be slightly wider and narrower than as reported in previous studies (Huo et al., 2018). For example, UV–vis absorption peaks provided sensitive λ^{max} values for the corresponding metal nanoparticles due to the small particle effect, which is hard to interpret in bulk compounds (Bindhu and Umadevi, 2014; González-Ballesteros et al., 2019). Recently, Hwang, (2021) studied the bioactive composition of DB aqueous extract. The extract contains higher total polyphenolics content (71.49 ± 0.01) mg/g and catechin content (638. 31 ± 39.62 µg/g) in DB plant. Also, the synthesis steps can be regulated by external physio-chemical factors including pH, metal salt concentration, and plant extract ratio, which have an important role in determining the size and dispersity.

3.2. Size, shape and elemental composition analysis of DB-AuNPs and DB-AgNPs using FESEM- EDX

The FESEM micrograph revealed that the synthesized gold and silver nanoparticles were mostly spherical, with a few rod and triangular shapes being noted in both samples (Fig. 3a and 3b (i-iii)). The gold and silver nanoparticles had size ranges of 5–25 nm and 10–45 nm, respectively. We also conducted an EDX analysis to confirm the elemental composition of the metal nanoparticles synthesized by the DB extract, as shown in Fig. 3a (iv-ix) and Fig. 3b (iv-x). The strong elemental signals were observed at 2.3 and 2.8 keV which confirmed the characteristic peak of gold and silver nanocrystalline, as shown in Fig. 3a (x) and Fig. 3b (xi) respectively. The elemental mapping of the DB-AuNPs and DB-AgNPs samples revealed that the selected area contains the maximum distribution element is gold (23 %) and silver (49 %) respectively (Fig. 3a and Fig. 3b). Also, some additional elements such as carbon, chloride, copper and oxygen were found in trace amounts in the samples, which presumably originated from the plant extract. Recently, the FESEM images clearly show that the plant extract *M. parviflora* synthesized AgNPs were mostly spherical. However, some irregular particles were found because of the composition of the synthesis medium and reaction parameters (Al-Otibi et al., 2021). The FESEM analysis of nanoparticle showed slightly agglomerated due to the centrifugation at high speed to separate nanoparticles from the colloidal solution. Thus, the organic layer acting as a capping agent was separated from the metal core, leading to particle agglomeration. The EDX analysis of the biosynthesized nanoparticles highlighted the presence of metallic nanoparticles and organic moieties. Also, the biosynthesized Au and Ag exhibited a strong signal of 2.95 and 2.67 keV in the nanoparticle samples and weaker signal of Cl and carbon, which originated from plant sources (Devi et al., 2016; Hussain et al., 2019). Mittal et al. (2012) found that *D. morbifera* (DM) extract synthesized metal nanoparticle samples showed a stronger signal of carbon than copper which indicates the impurities from the FESEM carbon grid used for sample preparation. In addition, the faint signals of chromium and oxygen were detected, which may have originated from biomolecules and certain components in the DM leaf extract. Furthermore, the elemental mapping analysis clearly showed the distribution of AuNPs and AgNPs located in the samples with different colors in selected electron micrograph regions.

3.3. TEM characterization of DB-AuNPs and DB-AgNPs

The DB-AuNPs and DB-AgNPs of size, morphology, and particle distribution nature of the nanoparticles at different magnifications using HR-TEM are presented in Fig. 4a and 4b. The DB synthesized Au and Ag nanoparticles were typically spherical, relatively uniform, and well dispersed. The particle size distribution diagram was drawn from Image J using TEM images of nanoparticles that calculated the average particle size of approximately 18 and 30 nm for gold and silver nanoparticles, respectively (Fig. 4a and 4b, (inserts)). The FFT of green synthesized DB-AuNPs and DB-AgNPs detected bright circular rings with a crystalline electron pattern. The characteristics of the indexing planes of (1 1 1), (2 0 0), (2 2 0) and (3 1 1) were noted to indicate the synthesized gold and silver nanoparticles were highly crystalline in nature. From TEM images that characterized the DB synthesized both AuNPs and AgNPs, the shapes of nanoparticles were highly spherical, and only a few irregular shapes were found in the FFT image of the internal spacing of the gold silver plane (1 1 1). Scimeca et al. (2018) reported that HR-TEM images of AuNPs synthesized
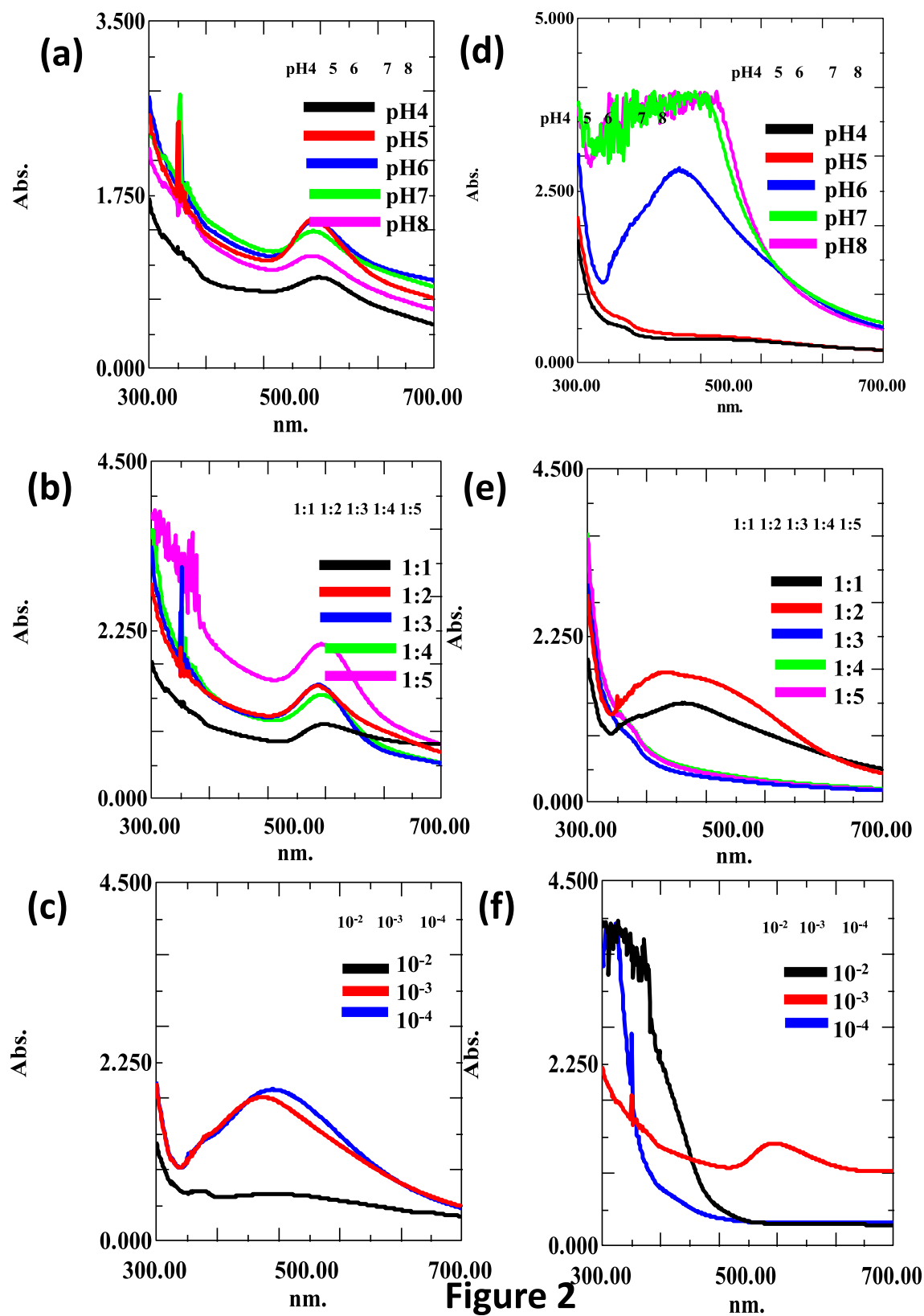
Fig. 2 Optimization of synthesis of DB-AuNPs and DB-AuNPs using different pH, plant extract, and metal salt concentrations. UV–vis absorbance spectra of DB synthesized gold (a-c) and silver nanoparticles (d-f) with different ranges of pH, ratio of plant extract, and metal ion concentrations, respectively, for 24 hrs.

(a)
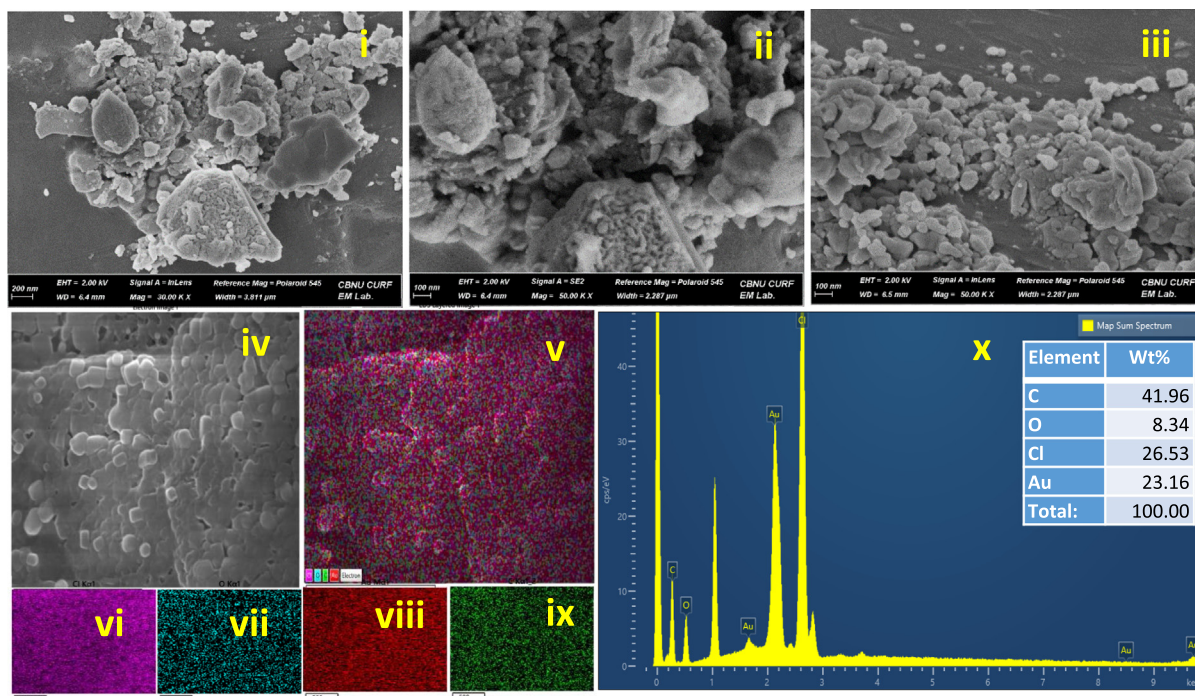
(b)
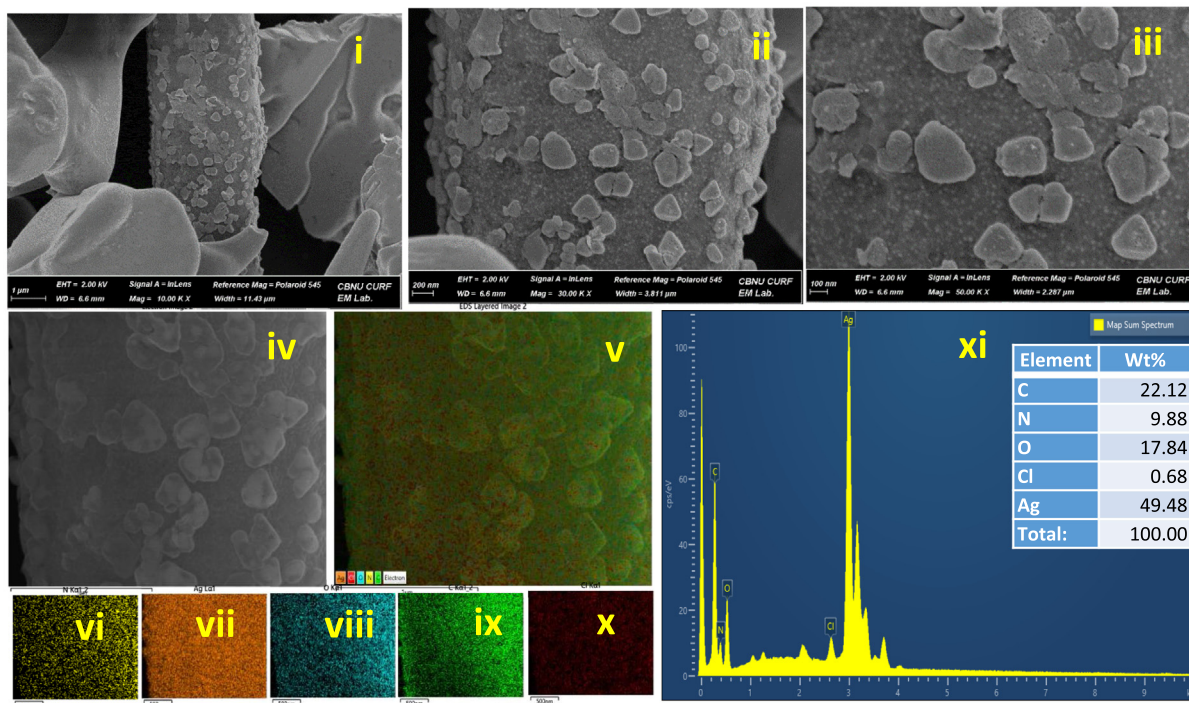
Fig. 3 Field Emission Scanning Electron Microscope image of DB synthesized AuNPs and AgNPs. (**a**) (i-iii) Size and morphology of the synthesized AuNPs with a scale bar of 100 nm. (iv-ix) Elemental mapping of purity and distribution analysis in selected electron micrograph region of gold nanoparticle sample. (x) Energy dispersive X-ray spectrum of biosynthesized AuNPs (inset table with composition of elements in wt.%). (**b**) (i-iii) Size and morphology of the biosynthesized AgNPs with a scale bar of 100 nm. (iv-x) Elemental mapping of purity and distribution analysis in selected electron micrograph region of silver nanoparticle sample. (xi) Energy dispersive X-ray spectrum of synthesized AgNPs (inset table with composition of elements in wt%).
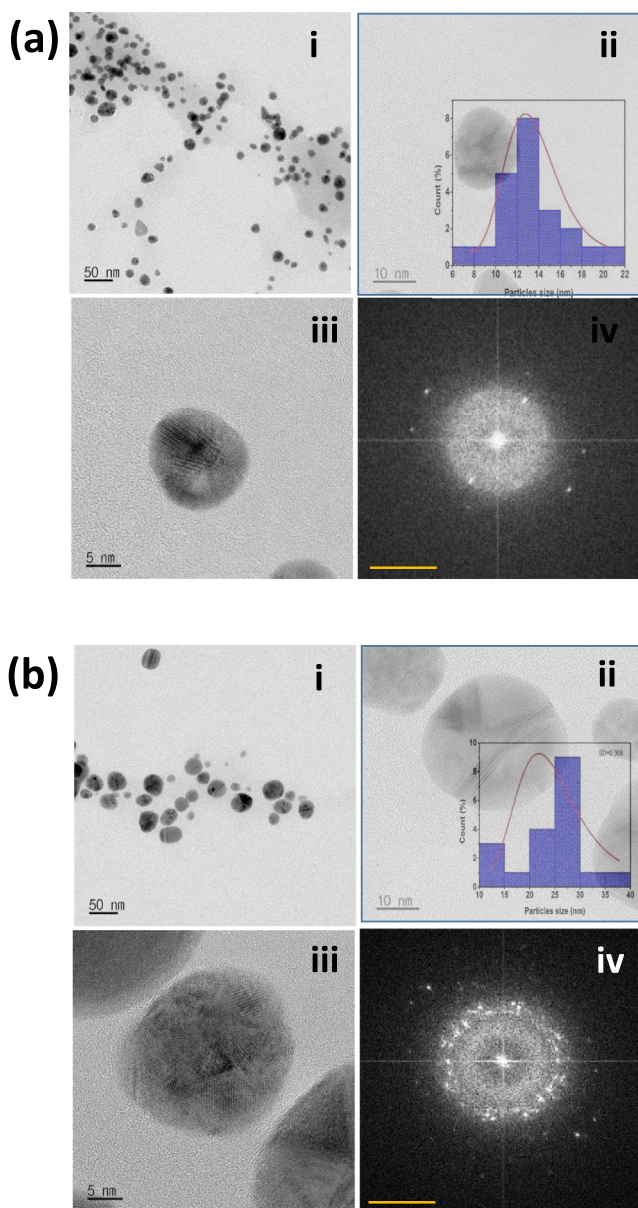
Fig. 4 Transmission Electron microscope images of DB synthesized AuNPs and AgNPs. (**a**) (i-iii) Shape and size of the synthesized AuNPs (scale bar: 50, 20 and 5 nm). (Inset: histogram diagram showing particle size distribution of synthesized gold NPs analysed using the ImageJ program. (iv) SAED pattern of the AuNPs. **b**) (i-iii) Shape and size of the synthesized AgNPs (scale bar: 50, 20 and 5 nm). (Inset: histogram diagram showing average size distribution of synthesized silver NPs analysed using the ImageJ program. (iv) SAED pattern of the AgNPs.

from plant extract showed highly ordered planar spacing, consistent with the internal spacing of metallic AuNPs. The size and shape of synthesized nanoparticles were measured and the AuNPs had a mean diameter of 15–34 nm with an almost spherical shape with smooth edges (Mohanta et al., 2017).

3.4. AFM topography of synthesized DB-AuNPs and DB-AgNPs

The surface topography of the DB synthesized AuNPs and AgNPs was analyzed using the AFM technique displayed in Fig. 5a and 5b. The 2D and 3D AFM images clearly showed the surface topology, height, roughness, and phases of the DB-AuNPs and DB-AgNPs, which indicated dense aggregates of spherical AuNPs and AgNPs with an average size of 25 and 30 nm respectively. The aggregation in AFM images was due to the sampling process in the AFM analysis. The nanoparticles samples were dropped onto a silica glass plate and allowed to dry to form a thin film of NPs, which may cause the NPs to appear clumped together. From 2D and 3D micrographs of the AuNPs, it was evident that the AgNPs are spherical with a few triangular, measured sizes ranging from 5 to 30 and 10–45 nm. The surface roughness of the gold and silver nanoparticles was calculated as 1.22 and 6.78 nm, respectively. Also, the agglomeration of the gold and silver nanoparticles was noticed, which was due to the sample coating preparation for AFM analysis (Alzharani et al., 2021). The results of our AFM analysis closely correlated with the TEM data discussed above.

3.5. FT-IR analysis of DB biosynthesized AuNPs and AgNPs

The function groups of secondary metabolites involved in the synthesis of DB-AuNPs and DB-AgNPs were identified using FTIR. Fig. 6i shows the FT-IR absorption spectra of DB AuNPs, AgNPs and DB plant extract alone. Fig. 6i shows the FT-IR absorption spectra of DB AuNPs, AgNPs and DB plant extract alone. The FT-IR spectrum of the DB extract showed major absorption peaks at 3396, 1711, 1599, 1438, 1234, 1149, 1094, 1040, 833, 608 and 547 cm^{-1} (Fig. 6 ii). The gold nanoparticles' major absorption peaks were found at 3221, 2260, 2027, 1609, 1479, 1195, 1109, 1037, 882 and 547 cm^{-1}, which indicates the different phytochemicals available in the samples. For AgNPs, we also found different absorption peaks at 3427, 2731, 2394, 1763, 1721, 1618, 1383 and 824 cm^{-1} (Fig. 6i). The AuNPs and AgNPs, whose broad bands were at 2394 and 547 cm^{-1}, completely disappeared, indicating that C—H and O—H were involved in the formation of metal nanoparticles. The weak band at 2700 cm^{-1} can be assigned to aliphatic C—H group stretching vibrations, which were present in DB-AgNPs but absent in DB-AuNPs and the plant extract. The transmittance signal at 1040 cm^{-1} showed the presence of reducing sugar and glycosidic bond C—O stretching vibration found in the DB extract. The mixture with metal salt and plant extract exhibited some additional functional groups (2260, 2027 and 2731, 2394 cm^{-1}) for gold and silver nanoparticles samples, which may have shifted from other unknown metabolites of the plant extract. The strong band at 1599 cm^{-1} corresponding to the C═C stretches (flavanones) and broad peaks at 3396 cm^{-1} indicated that N—H stretches (amide) were present in the plant samples. The prominent band at 1438 cm^{-1} may be attributed to the C—O stretching mode, indicating the presence of a carbonyl group. Also, the band at 1094 cm^{-1} corresponds to the presence of fatty
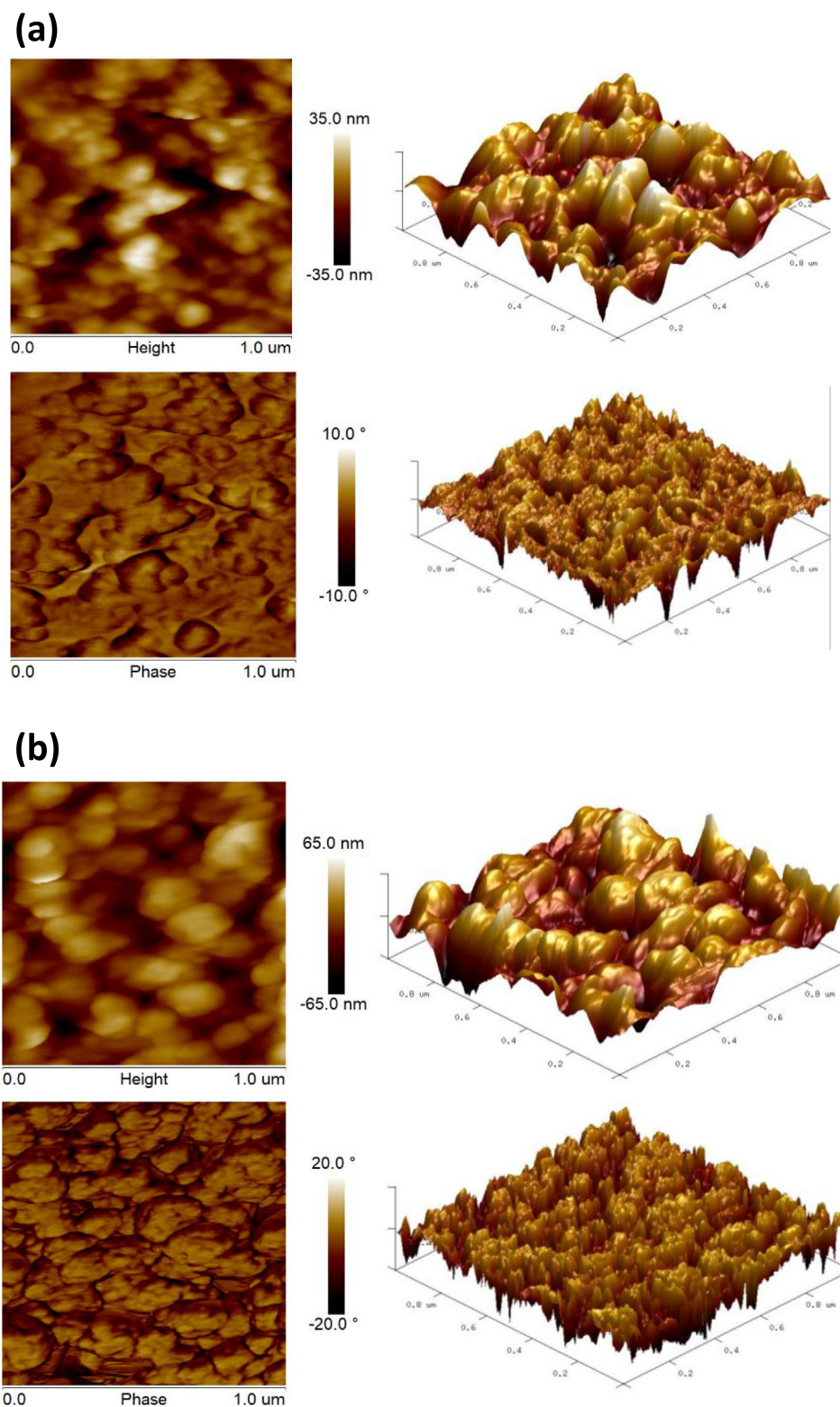
Fig. 5 AFM analysis of 2D and 3D structural views of DB synthesized (a) AuNPs and (b) AgNPs.

acids present in the DB extract. The IR spectra analysis demonstrates that different functional groups, including hydroxyl and carbonyl, are present in the DB aqueous extract. It suggests that the sugars and phenolic compounds could be used for the reduction and stabilization of the DB-AuNPs and DB-AgNPs samples.

FTIR spectrum analysis of the DB extract and biosynthesized nanoparticles exhibited similar intense peaks. Similarly, Agudelo et al. (2018) reported FT-IR characteristic bands at 3283 and 1637 cm^{-1}, which may be associated with a hydroxyl group (sucrose, glucose, fructose or glucoronic acid) which is responsible for the reduction process. The bands observed at

(a)

(b)
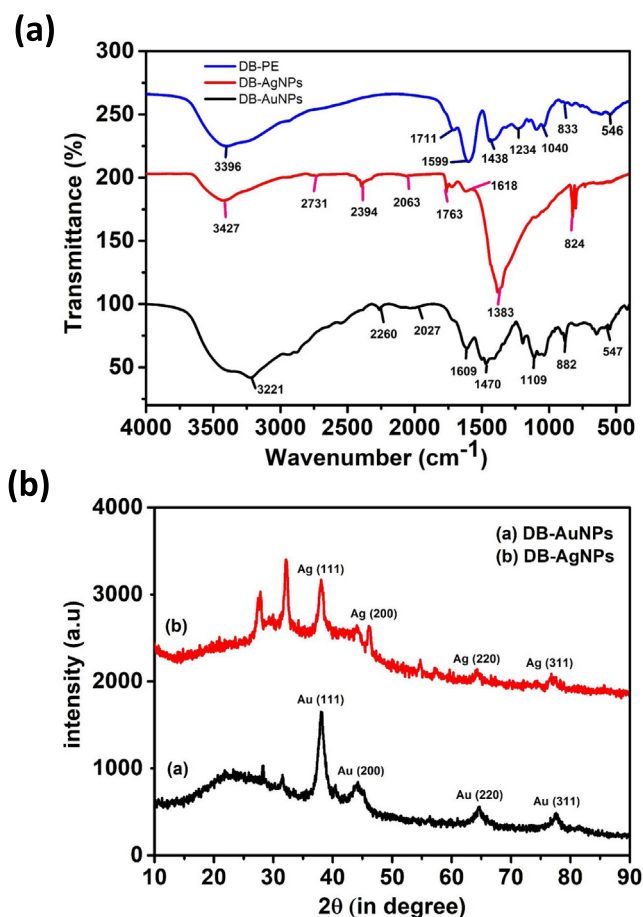
Fig. 6 (i) FTIR spectra of DB synthesized AuNPs, AgNPs, and DB PE for the identification of functional groups present on the nanoparticles' surface and in plant samples. (ii) Powder X-ray diffraction pattern analysis of biosynthesized gold and silver nanoparticles.

1638, 1296 and 657 cm^{-1}, assigned to C—C stretch, C—N amine stretch, and alkene stretch vibrations, were found in the SNL plant extract and nanoparticle synthesized samples (Vijilvani et al., 2020). In our results, we observed some peak splits and transmittance changes in the nanoparticles samples and plant extract, which also suggested that the plant compounds were involved in the reduction mechanisms. Lee et al. (2016) also found light shifting in the plant extract and nanoparticles samples, and they suggest that the carbonyl group (C—O) in the peel extract capped and stabilized the gold nanoparticles. The bands of C—H from *Garcinia mangostana* peel extract were spilt into two bands (2914 and 2845 cm^{-1}) suggesting that after the formation of AuNPs, the transmittance value was also altered. Kumari et al. (2020) reported that the band at 1043 cm^{-1} represents the O—H stretching of a polyphenolic group and the band at 832 cm^{-1} corresponds to the C—O stretch and the C—S stretch of aliphatic chloro compounds. In addition, the bands at 602 and 539 cm^{-1} might be a result of C—H stretching of aromatic compounds and –OH group of phenols. Therefore, the identified functional groups represent the metabolites present in the plant extract that regulate the nanoparticle synthesis in the green method.

3.6. XRD characterization of synthesized DB-AuNPs and DB-AgNPs

The powder XRD patterns of the biosynthesized DB gold and silver nanoparticles, as reported in Fig. 6ii. XRD diffraction peaks and planes were observed at 2θ = 38.2°, 44.6°, 66.3° and 77.5° corresponding to the (111), (200), (220) and (311) respectively, which reflected the gold nanocrystals presence in the DB synthesized AuNPs. Similarly, the XRD spectrum of DB-AgNPs confirmed that the nanoparticles were crystalline in nature, as shown by the obtained peak and planes of 2θ = 33.4°, 46.5°, 49.8° and 78.6° corresponding to (111), (200), (220) and (310), and these results were similar to the XRD pattern of AuNPs and AgNPs of previously published studies. In addition, the obtained XRD characteristic peaks conformed to standard ICDD data (JCPDS card no. 04–784, 89–3722 for gold and silver respectively). In addition, some addition peaks of face-centered cubic (fcc) gold and silver nanocrystals were observed at 28.1 and 41.3, which could indicate the presence of bioactive metabolites in the DB extract. The XRD diffractogram, in particular, revealed peaks of the (111), (200), and (311) planes, which corresponded to biosynthesized AuNPs and AgNPs using various plant extracts (Hemlata et al., 2020; Nadagouda et al., 2014). Similarly, Francis et al. (2017) claimed that the XRD patterns of AgNPs-SS and AuNPs-SS produced diffraction peaks corresponding to (111), (200), (220) and (311) planes of fcc crystal of nano-Ag and nano-Au and respective 2θ values at 37.42°, 44.16°, 64.44° and 77.29° (JCPDS file no. 4–0783) and 37.74°, 44.16°, 64.61° and 77.49° (JCPDS file no. 4–0784) respectively. Wang et al. (2016) also noted that, the crystalline structure of the biosynthesized AgNPs and AuNPs shows diffraction peaks at 38.19°, 44.34°, 64.48° and 77.46° are assigned to (111), (200), (220) and (311) lattice planes found to be identical to those reported for silver NPs, and XRD peaks at 38.09°, 44.40°, 64.56° and 77.60° set of lattice planes were observed that indexed to the (111), (200), (220) and (311) faces of gold NPs. There are no different crystal phases on the surface of the AuNPs and AgNPs, which indicates no impurities including, Au^{3+} and Ag$^+$ ions within the plant extract mixture.

3.7. Antimicrobial activity of biosynthesized DB-AuNPs and DB- AgNPs

Fig. 7 shows the antibacterial activity of DB-AuNPs, DB-AgNPs and DB-PE using agar disc diffusion method. DB-AuNPs, DB-AgNPs, and DB-PE were tested against livestock pathogens including *Salmonella typhi* (G-), *Salmonella enteritidis* (G-), *Salmonella derby* (G-), *E. coli* (G-), *Yersinia enterocolitica* (G-), *Yersinia pseudotuberculosis* (G-), and *Clostridium difficile* (G +). The DB synthesized AgNPs showed the highest inhibitory activity against *Y. pseudotuberculosis* (20 ± 3 mm) and moderate inhibitory activity against *S. typhi* (9 ± 3 mm), *S. enteritidis* (11 ± 3 mm), *S. derby* (11 ± 3 mm), *E. coli* (11 ± 3 mm), *Y. enterocolitica* (11 ± 3 mm), and *C. difficile* (11 ± 3 mm). The DB synthesized AuNPs shows strong inhibitory activity against *Y. pseudotuberculosis* (20 ± 3 mm) and moderate inhibition of *S. derby* (14 ± 3 mm) and weak activity against *E. coli*. In addition, the AuNPs demonstrated no bactericidal activity against *Salmonella sp* and *Y. enterocolitica*. The antibacterial activity of DB-AgNPs had a higher
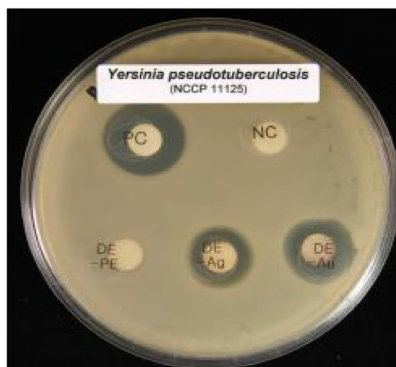
Yersinia pseudotuberculosis
NCCP 11125
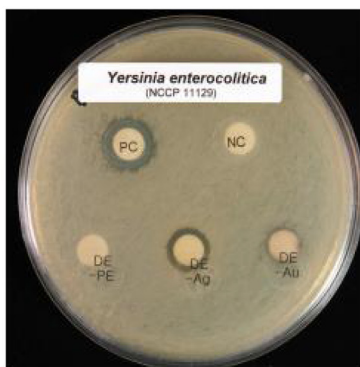
Yersinia enterocolitica
NCCP 11129
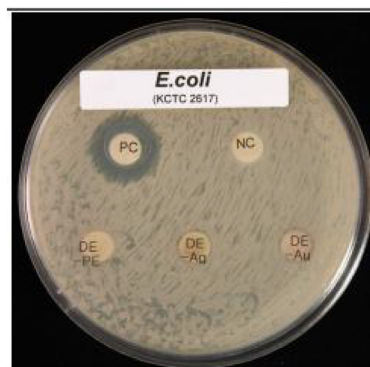
E.coli
KCTC 2617
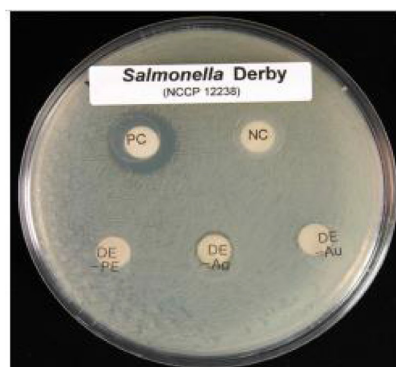
Salmonella Derby
NCCP 12238

Salmonella enteritidis
NCCP 30939

Salmonella Typhimurium
NCCP 10438

Clostridium difficile
JCM 1296

Candida glabrata
NCCP 30939
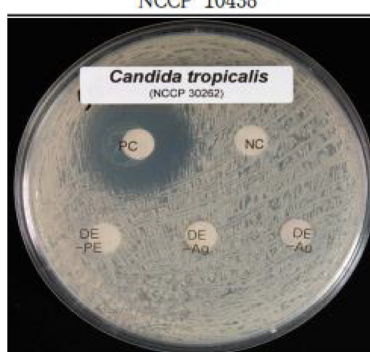
Candida tropicalis
NCCP 30262
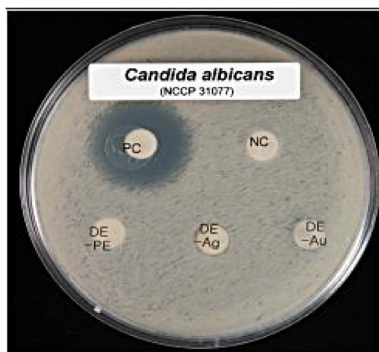
Candida albicans
NCCP 31077

Table 1 Zone of inhibition of biosynthesized DB-AuNPs, DB-AgNPs, and DB-PE tested against different gram negative and gram negative pathogenic livestock bacteria and fungi. Antioxidant activities of DB-AuNPs DB-AgNPs and DB-PE were calculated using the DPPH method.

Components	Antibacterial activity in zone of inhibition (mm)							Antifungal activity (mm)			Antioxidant activity (%)
	ST	SE	SD	EC	YE	YS	CD	CA	CT	CG	DPPH
DB-PE	–	–	–	–	–	–	–	–	–	–	39
DB-AuNPs	–	–	+	w	–	+ + +	+	–	–	–	41
DB-AgNPs	+	+	+	+	+	+ +	–	w	w	w	43
Ampicillin	+ + +	+ + +	+ +	+ +	+ +	+ +	NA	NA	NA	NA	NA
Gentamycin	NA	NA	NA	NA	NA	NA	+ +	+ +	+ + +	+ + +	NA
Vitamin C	NA	NA	NA	NA	NA	NA	NA	NA	NA	NA	63.5

(Note: + + +, ≥ 14–20 mm; + +, ≥ 12–14 mm; +, ≥ 9 mm; w (weak), less than 9 mm; -, no inhibition, NA, Not applicable; Abbreviations: ST-*Salmonella typhi*, SE-*Salmonella enteritidis*, SD-*Salmonella derby*, EC-*Escherichia coli*, YE-*Yersinia enterocolitica*, YP-*Yersinia pseudotuberculosis*, CD-*Clostridium difficile*, CA-*Candida albicans*, CT-*Candida tropicalis*, and CG-*Candida glabrata*).

inhibition zone in gram negative strains compared to the DB AuNPs. It is because of the NPs' larger surface area and binging ability to attach to the cell membrane of the bacterial cell wall. We also noticed zone of inhibition differences that may be due to the variation in the resistance of the pathogenic strains to the plant derived nanoparticles. From our findings, increasing the concentration of nanoparticles can be effective against resistant bacterial strains. The zone of inhibition values of plant extract and DB synthesized nanoparticles are presented in Table 1. Both DB-AuNPs and DB-AgNPs showed good inhibition against gram negative bacteria (*Y. pseudotuberculosis*) with a maximum inhibition zone of (14–20 mm) and (12–14 mm) respectively. But, the DB-AgNPs showed positive inhibitory activity for all gram positive and gram negative bacteria compared to DB-AuNPs. The DB-AuNPs sample had no antibacterial effect against *S. typhi*, *S. enteritidis*, or *Y. entereocolitica* strains, which could be attributed to differences in cell wall components in strains resistant to the synthesized gold nanoparticles. 20 μL of AuNPs showed significant activity against gram positive bacteria (*C. difficile*) and gram negative bacteria (*Y. enterocolitica* and *E.coli*). The same concentration of DB-AgNPs also showed potent antibacterial activity against a wide range of pathogenic strains, including *C. difficile*, *Y. enterocolitica*, *Salmonella derby*, *Salmonella typhi*, *Yersinia pseudotuberculosis* and *E.coli*. The main reasons for the bactericidal effects of metallic gold and silver nanoparticles were pathogenic bacterial protein degradation and DNA replication inhibition (Balouiri et al., 2016). Moreover, the AgNPs interacted effectively with thiol (-S─O) that present in bacterial cell membrane proteins, resulting in suppression of protein synthesis and the multiplication and growth of bacteria. Similarly, oxygen is associated with silver and reacts with sulfhydryl (-S─H) groups on the cell wall of bacteria, resulting in sulphur atoms to form, which block cellular respiration, leading to cell death (Feng et al., 2000; Gopinath et al., 2016). Therefore, the DB-AgNPs possessed a higher degree of antibacterial properties than the Au nanoparticles. In our

study, the DB synthesized AgNPs had enhanced activity against gram negative bacteria compared to DB-AuNPs. The DB-AgNPs clearly impacted the lethality of gram negative bacteria even at lower concentrations (20 μL), whereas gram positive bacteria required higher concentrations to control the growth of bacteria (Tippayawat et al., 2016).

Fig. 7 shows the fungicidal effect of DB-AuNPs and DB-AgNPs against *Candida* species using the agar disc diffusion method. The DB-AgNPs showed less activity against *Candida* fungal strains at a 20 μL concentration. The inhibition zone was calculated as less than 9 mm for selected three strains such as *C. albicans*, *C. tropicalis* and *C. glabrata*. All Candida pathogens were unaffected by the DB-AuNPs. The nanoparticles' size, shape, and surface molecules are responsible for the antimicrobial activity of metal nanoparticles. In this study, DB-AgNPs exhibited significant antifungal activity, against *C. albicans*, *C. tropicalis* and *C. glabrata*. The DB-AuNPs did not show any response to the *Candida* sp. Thus, the antifungal activity is majorly different between the cell walls of these pathogens and considering the active ingredients available on the surface of the synthesized nanoparticles (Rónavári et al., 2018).

3.8. Antioxidant analysis of DB-AuNPs and DB-AgNPs

DPPH free radical scavenging activities of DB plant extract, DB-AuNPs, DB-AgNPs and standard drug are presented in Table 1. The antioxidant profile of plant extract and synthesized NPs increased depending on the concentration increases, indicating that antioxidant potential is dose dependent. Results showed that the highest free radical scavenging was observed in DB-AuNPs and DB-AgNPs at 5 mg/ml. The percentage of DPPH antioxidant potential was calculated for DB-PE, DB-AuNPs and DB-AgNPs as 43 %, 41 % and 44 % respectively. We also observed that the DB synthesized AuNPs and AgNPs exhibited good free scavenging activity in dose dependent manner. DPPH free radical scavenging percentage

Fig. 7 Antimicrobial test of agar plates containing biosynthesized DB-AuNPs, DB-AgNPs, and DB-PE impregnated discs (20 μL); diameter of inhibition zone tested against gram positive and gram negative pathogenic livestock bacteria, and *Candida* sp. Ampicillin (20 μL) was used as control for antibacterial assay and gentamycin (20 μL) was used control for *Candida* sp. antifungal test.

calculated for the lowest concentration of DB-AuNPs and DB-AgNPs was 41 % and 43 %, respectively, and the scavenging percentage increased as the concentration increased to 5 mg/ml. However, the standard drug vitamin C shows higher activity (63.5 %) than the DB mediated AuNPs and AgNPs. González-Ballesteros et al. (2019) reported results were similar

to our observation of higher antioxidant activity in AgNPs compared with AuNPs, as Ag act as good reducing compounds, which can lose electrons more easily than gold metal NPs. In addition, the proton donating capacity of SEEr-AuNPs was noticeably higher than that of SEEr-AgNPs, which means AgNPs can be potent antioxidants compared to
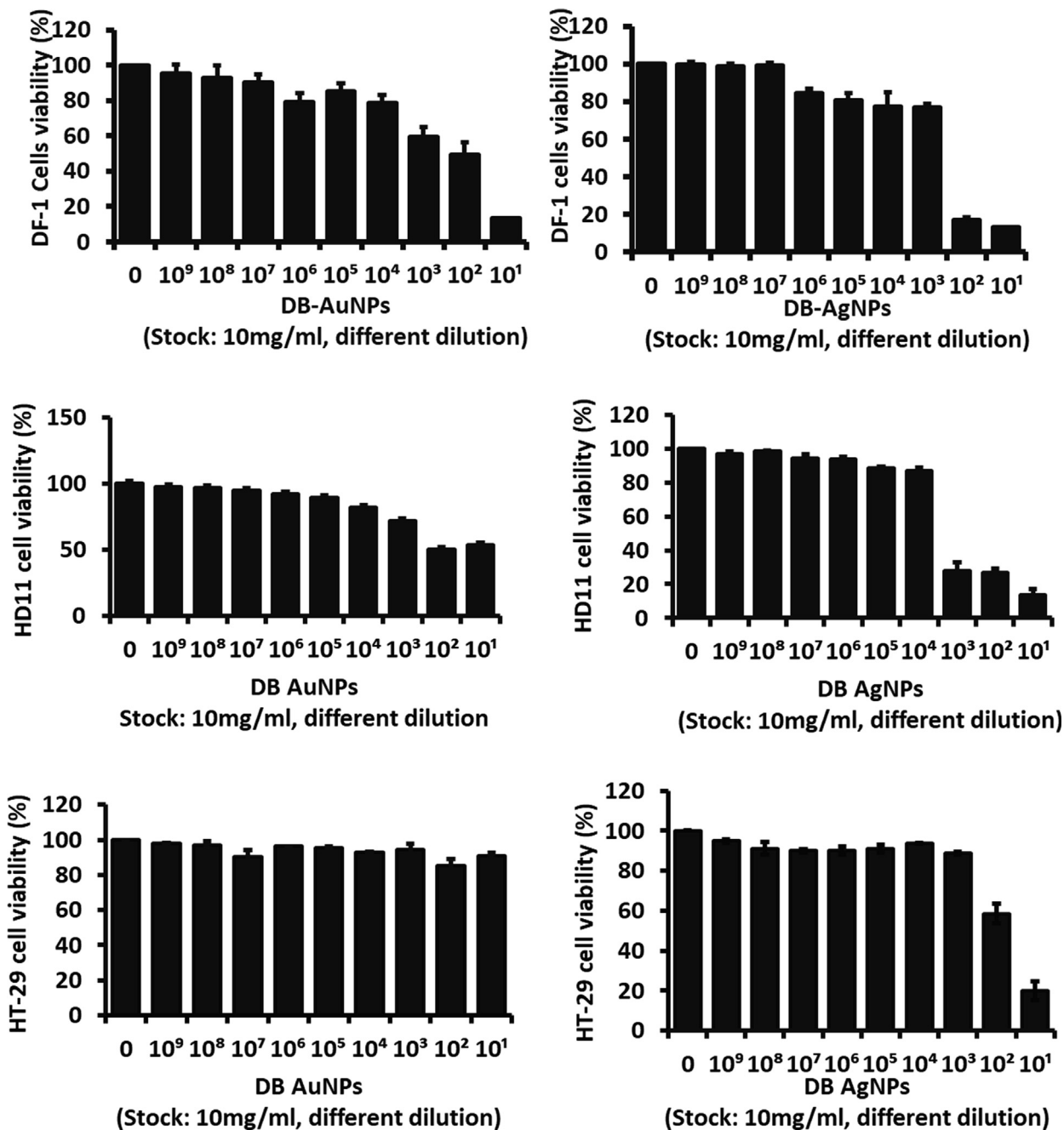
Fig. 8 Cell cytotoxicity effects of DB synthesized gold and silver nanoparticles on chicken fibroblast cells (DF-1), chicken macrophage (HD11), and human colon cancer cells (HT-29) after 24 hr treatment. Results show the cell viability percentage of groups treated with nanoparticles compared with control samples *(p ≤ 0.005). (Stock concentration was 10 mg/ml, diluted into $10^{-1} - 10^{-9}$ = 1 mg/ml – 0.01 pg/ml).
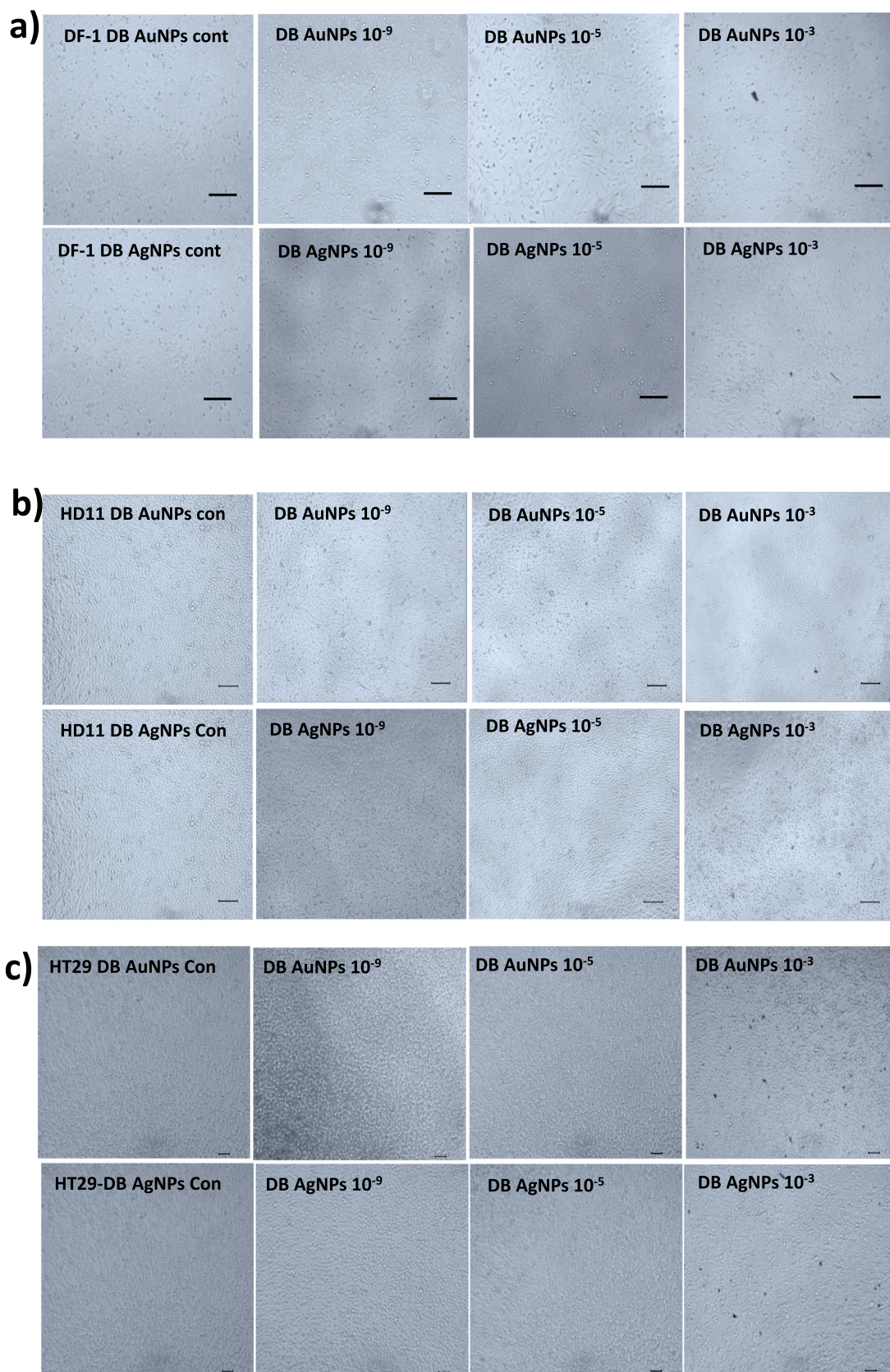
Fig. 9 Cells were treated with different concentrations of biosynthesized DB-AuNPs and DB-AgNPs for 24 hr. Morphological changes were observed in the nanoparticle-treated cells and control cells using a light microscope. (a) DF1 cells, (b) HD11 cells, and (c) HT-29 cells treated with different dilutions of DB synthesized AuNPs and AgNPs. (Stock concentration was 10 mg/ml, diluted into $10^{-1} - 10^{-9}$ dilution = 1 mg/ml – 0.01 pg/ml).

other metal NPs. However, the scavenging potential of BO-AgNPs was lower than that of the ascorbic acid standard (Ansar et al., 2020).

3.9. Cell cytotoxicity analysis by WST-1 assay using DB synthesized AuNPs and AgNPs

The cytotoxicity effect of the biosynthesized DB-AuNPs and DB-AgNPs was analyzed against chicken embryonic fibroblast (DF-1), chicken macrophage (HD 11) and human colon cancer (HT-29) cells. The in vitro cytotoxicity results were conducted with different concentrations of DB-AuNPs and DB-AgNPs from (10^{-1} to 10^{-9}) dilution for 24 hr as displayed in Fig. 8. These results suggest that cell viability decreased at maximum concentrations (10^{-1} and 10^{-2}) of DB-AgNPs in selected cell lines (DF-1, HD 11 and HT-29). The cell viability percentage in DB-AgNPs treated chicken cells and human cancer cells was less than 30 % at (10–1) and (10–2). Also, the DB-AuNPs showed less cytotoxicity against chicken cell lines at a moderate concentration, however, cell viability was measured at 90 %, even at higher concentrations of DB synthesized AuNPs. In addition, we found that cellular viability was more than 80 % for these cell lines at a concentration of (10–4 to 10^{-9}) dilution of both DB-AuNPs and DB-AgNPs, and thus safe for the cells. The cytotoxicity study revealed that the DB-PE synthesized AuNPs and AgNPs had excellent cell viability even at higher concentrations for chicken and human cell lines. Also, the microphotographic images clearly demonstrated that the cell numbers were reduced and morphology was altered when treated with the maximum concentration of AuNPs and AgNPs (Fig. 9). The medium and lower concentrations found no changes in the cell number, structure, or viability of the cells. In this case, the DB green synthesized nanoparticle exposure may be less harmful for the cell lines such as DF-1, HD 11 and HT-29. However, the higher concentration of DB-AuNPs and DB-AgNPs may cause cell death in the chicken cells because of their surface functionalization and size characteristics. In this study, the maximum concentration (10^{-1}–10^{-2}) of DB-AuNPs and DB-AgNPs were tested, and we found that both of the DB synthesized AuNPs and AgNPs did not reduce the cell viability even at moderate and higher concentrations for 24 hrs. The DB-AuNPs and DB-AgNPs showed more than 80 % viability at 10^{-4} to 10^{-9} dilution. The DB synthesized AuNPs and AgNPs were showed lower cell viability by approximately 20 % at higher concentrations (10^{-1} to 10^{-3}) in chicken cell and colon cancer cells.

The synthesized metallic nanoparticles contain various bioactive metabolites on the surface. Because of the green components, they are supposed to have lower toxicity against colon and breast cancer cell lines (Lee et al., 2015; Loutfy et al., 2015; Venugopal et al., 2017). Recently, Cao et al. (2021) reported that L-AgNPs was detected with less cytotoxicity against A549 lung cancer cells. The L-AgNPs exposed A549 cells showed a 98 % survival rate. Thus, the L-AgNPs have very low cell toxicity and are more suitable as antibacterial agents. Similarly, Markus et al. (2017) suggest that DH-AuNPs are used at a 5 g/ml concentration to treat the RAW 264.7 cells in in vitro. The RAW 264.7 cell line did not exhibit cell death at this concentration and continued to proliferate. On the other hand, Park et al. (2011) observed that the silver nanoparticles showed excellent cytotoxicity against the A431 osteosarcoma cell line with an

optimal concentration. The cytotoxic effect of gold and silver metallic nanoparticles is dependent on the nature of size, shapes, large surface to volume ration, attachment and permeability ability into cells (Patil and Kim, 2017). In our study, the viability of cells did not significantly decrease at greater concentrations (10^{-4} dilution). Therefore, these results indicate that DB-AuNPs and AgNPs may not exhibit cytotoxicity against chicken and colon cancer cells at this condition. As a result, the synthesized nanoparticle could be used in other biomedical applications such as drug delivery and molecular imaging for disease diagnosis.

4. Conclusion

Gold and silver ions were effectively reduced and capped by aqueous *D. brittonii* extract via biosynthesis approaches. The synthesized DB-AuNPs and DB-AgNPs were monodispersed in spherical shapes with size ranges from 5 to 25 nm and 10–45 nm. XRD analysis confirmed that the DB-AuNPs and DB-AgNPs were crystalline in nature, with an FCC structure. The presence of functional groups such as hydroxyl, aldehyde, alkene, and amines in the plant extract is clearly indicated by the FT-IR spectra, which could be responsible for the reduction and stabilization of the metal nanoparticle found that the DB mediated AuNPs and AgNPs demonstrated potent antibacterial activity against livestock pathogenic microorganisms and also that these nanoparticles were capped by natural phyto-compounds, making them less toxic to the host when used at high concentration. In addition, the DB-AuNPs and DB-AgNPs exhibited less cytotoxicity against chicken fibroblast, macrophage cell lines, and human colon cancer cells. Hence, the biosynthesized gold and silver nanoparticles using DB extract could be useful as adjuvants in vaccine development, and as antimicrobial agents to control pathogenic infection in the livestock industry.

Declaration of Competing Interest

The authors declare that they have no known competing financial interests or personal relationships that could have appeared to influence the work reported in this paper.

Acknowledgement

Funding

References

Agudelo, W., Montoya, Y., Bustamante, J., 2018. Using a non-reducing sugar in the green synthesis of gold and silver nanoparticles by the chemical reduction method. DYNA 85, 69–78. https://doi.org/10.15446/dyna.v85n206.72136.

Alabdallah, N.M., Hasan, M.M., 2021. Plant-based green synthesis of silver nanoparticles and its effective role in abiotic stress tolerance in crop plants. Saudi J. Biol. Sci. 28, 5631–5639. https://doi.org/10.1016/J.SJBS.2021.05.081.

Al-Otibi, F., Perveen, K., Al-Saif, N.A., Alharbi, R.I., Bokhari, N.A., Albasher, G., Al-Otaibi, R.M., Al-Mosa, M.A., 2021. Biosynthesis of silver nanoparticles using Malva parviflora and their antifungal activity. Saudi J. Biol. Sci. 28, 2229–2235. https://doi.org/10.1016/J.SJBS.2021.01.012.

Alzharani, S., Astudillo-calderón, S., Pintos, B., Pérez-urria, E., Manzanera, J.A., Martín, L., Gomez-garay, A., 2021. Role of synthetic plant extracts on the production of silver-derived nanoparticles. Plants 10. https://doi.org/10.3390/plants10081671.

Annamalai, A., Christina, V.L.P., Sudha, D., Kalpana, M., Lakshmi, P.T.V., 2013. Green synthesis, characterization and antimicrobial activity of Au NPs using Euphorbia hirta L. leaf extract. Colloids Surf. B. Biointerfaces 108, 60–65. https://doi.org/10.1016/J.COLSURFB.2013.02.012.

Ansar, S., Tabassum, H., Aladwan, N.S.M., Naiman Ali, M., Almaarik, B., AlMahrouqi, S., Abudawood, M., Banu, N., Alsubki, R., 2020. Eco friendly silver nanoparticles synthesis by Brassica oleracea and its antibacterial, anticancer and antioxidant properties. Sci. Rep. 10, 1–12. https://doi.org/10.1038/s41598-020-74371-8.

Arvizo, R., Bhattacharya, R., Mukherjee, P., 2010. Gold nanoparticles: opportunities and challenges in nanomedicine. Expert Opin. Drug Deliv. 7, 753–763. https://doi.org/10.1517/17425241003777010.

Balouiri, M., Sadiki, M., Ibnsouda, S.K., 2016. Methods for in vitro evaluating antimicrobial activity: a review. J. Pharm. Anal. 6, 71–79. https://doi.org/10.1016/J.JPHA.2015.11.005.

Bamal, D., Singh, A., Chaudhary, G., Kumar, M., Singh, M., Rani, N., Mundlia, P., Sehrawat, A.R., 2021. Silver nanoparticles biosynthesis, characterization, antimicrobial activities, applications, cytotoxicity and safety issues: an updated review. Nanomaterials 11. https://doi.org/10.3390/nano11082086.

Bilgic, E., Tuncel, N., Koca, T., 2021. Radio-sensitivity on MCF-7 cells of silver nanoparticles synthesized by Silybum marianum. Inorg. Nano-Metal Chem. https://doi.org/10.1080/24701556.2021.1987460.

Bindhu, M.R., Umadevi, M., 2014. Silver and gold nanoparticles for sensor and antibacterial applications. Spectrochim. Acta - Part A Mol. Biomol. Spectrosc. 128, 37–45. https://doi.org/10.1016/j.saa.2014.02.119.

Botteon, C.E.A., Silva, L.B., Ccana-Ccapatinta, G.V., Silva, T.S., Ambrosio, S.R., Veneziani, R.C.S., Bastos, J.K., Marcato, P.D., 2021. Biosynthesis and characterization of gold nanoparticles using Brazilian red propolis and evaluation of its antimicrobial and anticancer activities. Sci. Rep. 11, 1–16. https://doi.org/10.1038/s41598-021-81281-w.

Cao, X., Zhu, L., Bai, Y., Li, F., Yu, X., 2021. Green one-step synthesis of silver nanoparticles and their biosafety and antibacterial properties. http://mc.manuscriptcentral.com/tgcl 15, 26–32. https://doi.org/10.1080/17518253.2021.2018506

Das, S., Langbang, L., Haque, M., Belwal, V.K., Aguan, K., Singha Roy, A., 2021. Biocompatible silver nanoparticles: an investigation into their protein binding efficacies, anti-bacterial effects and cell cytotoxicity studies. J. Pharm. Anal. 11, 422–434. https://doi.org/10.1016/J.JPHA.2020.12.003.

Devi, T.B., Ahmaruzzaman, M., Begum, S., 2016. A rapid, facile and green synthesis of Ag@AgCl nanoparticles for the effective reduction of 2,4-dinitrophenyl hydrazine. New J. Chem. 40, 1497–1506. https://doi.org/10.1039/C5NJ02367J.

Doan, V.D., Luc, V.S., Nguyen, T.L.H., Nguyen, T.D., Nguyen, T.D., 2020. Utilizing waste corn-cob in biosynthesis of noble metallic nanoparticles for antibacterial effect and catalytic degradation of contaminants. Environ. Sci. Pollut. Res. 27, 6148–6162. https://doi.org/10.1007/s11356-019-07320-2.

Donga, S., Bhadu, G.R., Chanda, S., 2020. Antimicrobial, antioxidant and anticancer activities of gold nanoparticles green synthesized using Mangifera indica seed aqueous extract. Artif. Cells, Nanomed. Biotechnol. 48, 1315–1325. https://doi.org/10.1080/21691401.2020.1843470.

Erdogan, O., Abbak, M., Demirbolat, G.M., Birtekocak, F., Aksel, M., Pasa, S., Cevik, O., 2019. Green synthesis of silver nanoparticles via Cynara scolymus leaf extracts: the characterization, anticancer potential with photodynamic therapy in MCF7 cells. PLoS One 14, 1–15. https://doi.org/10.1371/journal.pone.0216496.

Feng, Q.L., Wu, J., Chen, G.Q., Cui, F.Z., Kim, T.N., Kim, J.O., 2000. A mechanistic study of the antibacterial effect of silver ions on Escherichia coli and Staphylococcus aureus. https://doi.org/10.1002/1097-4636

Francis, S., Joseph, S., Koshy, E.P., Mathew, B., 2017. Microwave assisted green synthesis of silver nanoparticles using leaf extract of elephantopus scaber and its environmental and biological applications. https://doi.org/10.1080/21691401.2017.1345921 46, 795–804. https://doi.org/10.1080/21691401.2017.1345921

González-Ballesteros, N., Diego-González, L., Lastra-Valdor, M., Rodríguez-Argüelles, M.C., Grimaldi, M., Cavazza, A., Bigi, F., Simón-Vázquez, R., 2019. Immunostimulant and biocompatible gold and silver nanoparticles synthesized using the: Ulva intestinalis L. aqueous extract. J. Mater. Chem. B 7, 4677–4691. https://doi.org/10.1039/c9tb00215d.

Gopinath, K., Kumaraguru, S., Bhakyaraj, K., Mohan, S., Venkatesh, K.S., Esakkirajan, M., Kaleeswarran, P., Alharbi, N.S., Kadaikunnan, S., Govindarajan, M., Benelli, G., Arumugam, A., 2016. Green synthesis of silver, gold and silver/gold bimetallic nanoparticles using the Gloriosa superba leaf extract and their antibacterial and antibiofilm activities. Microb. Pathog. 101, 1–11. https://doi.org/10.1016/j.micpath.2016.10.011.

Hemlata, Meena, P.R., Singh, A.P., Tejavath, K.K., 2020. Biosynthesis of Silver Nanoparticles Using Cucumis prophetarum Aqueous Leaf Extract and Their Antibacterial and Antiproliferative Activity against Cancer Cell Lines. ACS Omega 5, 5520–5528. https://doi.org/10.1021/acsomega.0c00155

Huo, Y., Singh, P., Kim, Y.J., Soshnikova, V., Kang, J., Markus, J., Ahn, S., Castro-Aceituno, V., Mathiyalagan, R., Chokkalingam, M., Bae, K.S., Yang, D.C., 2018. Biological synthesis of gold and silver chloride nanoparticles by Glycyrrhiza uralensis and in vitro applications. Artif. Cells, Nanomedicine Biotechnol. https://doi.org/10.1080/21691401.2017.1307213.

Hussain, A., Alajmi, M.F., Khan, M.A., Pervez, S.A., Ahmed, F., Amir, S., Husain, F.M., Khan, M.S., Shaik, G.M., Hassan, I., Khan, R.A., Rehman, M.T., 2019. Biosynthesized silver nanoparticle (AgNP) from pandanus odorifer leaf extract exhibits anti-metastasis and anti-biofilm potentials. Front. Microbiol. 10, 1–19. https://doi.org/10.3389/fmicb.2019.00008.

Hwang E. 2021. (Doctoral Dissertation). A study on the valuable candidates for the Bio-Industry through the exploration of bioactive substances derived from succulents: Sedeveria, Senecia and Aeonium species. Hoseo University Library, Cheonan, Korea, p: 1-80.

Kalpana, D., Han, J.H., Park, W.S., Lee, S.M., Wahab, R., Lee, Y.S., 2019. Green biosynthesis of silver nanoparticles using Torreya nucifera and their antibacterial activity. Arab. J. Chem. 12, 1722–1732. https://doi.org/10.1016/J.ARABJC.2014.08.016.

Kharat, S.N., Mendhulkar, V.D., 2016. Synthesis, characterization and studies on antioxidant activity of silver nanoparticles using Elephantopus scaber leaf extract. Mater. Sci. Eng. C Mater. Biol. Appl. 62, 719–724. https://doi.org/10.1016/J.MSEC.2016.02.024.

Kim, H., Jeon, E.H., Park, B.C., Kim, S.J., 2019. Dudleya brittonii extract promotes survival rate and M2-like metabolic change in porcine 3D4/31 alveolar macrophages. Asian-Australasian J. Anim. Sci. 32, 1789–1800. https://doi.org/10.5713/ajas.19.0251.

Koul, B., Poonia, A.K., Yadav, D., Jin, J.O., 2021. Microbe-mediated biosynthesis of nanoparticles: applications and future prospects. Biomolecules 11. https://doi.org/10.3390/biom11060886.

Kumar, V.G., Gokavarapu, S.D., Rajeswari, A., Dhas, T.S., Karthick, V., Kapadia, Z., Shrestha, T., Barathy, I.A., Roy, A., Sinha, S., 2011. Colloids and surfaces B : biointerfaces facile green synthesis of gold nanoparticles using leaf extract of antidiabetic potent Cassia auriculata. Colloids Surf. B Biointerfaces 87, 159–163. https://doi.org/10.1016/j.colsurfb.2011.05.016.

Kumari, R., Saini, A.K., Kumar, A., Saini, R.V., 2020. Apoptosis induction in lung and prostate cancer cells through silver nanoparticles synthesized from Pinus roxburghii bioactive fraction. J. Biol. Inorg. Chem. 25, 23–37. https://doi.org/10.1007/S00775-019-01729-3.

Kuppusamy, P., Yusoff, M.M., Maniam, G.P., Govindan, N., 2016. Biosynthesis of metallic nanoparticles using plant derivatives and their new avenues in pharmacological applications – an updated report. Saudi Pharm. J. 24. https://doi.org/10.1016/j.jsps.2014.11.013.

Lee, K.D., Palaniselvam Kuppusamy, ●, Da, ●, Kim, H., Govindan, N., Gaanty, ●, Maniam, P., Ki, ●, Choi, C., 2088. Forage Crop Lolium multiflorum Assisted Synthesis of AgNPs and Their Bioactivities Against Poultry Pathogenic Bacteria in In Vitro. Indian J. Microbiol. 58. https://doi.org/10.1007/s12088-018-0755-8.

Lee, K.D., Nagajyothi, P.C., Sreekanth, T.V.M., Park, S., 2015. Eco-friendly synthesis of gold nanoparticles (AuNPs) using Inonotus obliquus and their antibacterial, antioxidant and cytotoxic activities. J. Ind. Eng. Chem. 26, 67–72. https://doi.org/10.1016/J.JIEC.2014.11.016.

Loutfy, S.A., Al-Ansary, N.A., Abdel-Ghani, N.T., Hamed, A.R., Mohamed, M.B., Craik, J.D., Salah Eldin, T.A., Abdellah, A.M., Hussein, Y., Hasanin, M.T.M., Elbehairi, S.E.I., 2015. Anti-proliferative activities of metallic nanoparticles in an in vitro breast cancer model. Asian Pacific J. Cancer Prev. 16, 6039–6046. https://doi.org/10.7314/APJCP.2015.16.14.6039.

Manikandan, R., Manikandan, B., Raman, T., Arunagirinathan, K., Prabhu, N.M., Jothi Basu, M., Perumal, M., Palanisamy, S., Munusamy, A., 2015. Biosynthesis of silver nanoparticles using ethanolic petals extract of Rosa indica and characterization of its antibacterial, anticancer and anti-inflammatory activities. Spectrochim. Acta. A. Mol. Biomol. Spectrosc. 138, 120–129. https://doi.org/10.1016/J.SAA.2014.10.043.

Markus, J., Wang, D., Kim, Y.J., Ahn, S., Mathiyalagan, R., Wang, C., Yang, D.C., 2017. Biosynthesis, characterization, and bioactivities evaluation of silver and gold nanoparticles mediated by the roots of Chinese herbal Angelica pubescens maxim. Nanoscale Res. Lett. 12. https://doi.org/10.1186/s11671-017-1833-2.

Mat Yusuf, S.N.A., Che Mood, C.N.A., Ahmad, N.H., Sandai, D., Lee, C.K., Lim, V., 2020. Optimization of biogenic synthesis of silver nanoparticles from flavonoid-rich Clinacanthus nutans leaf and stem aqueous extracts: biogenic synthesis of C. nutans AgNPs. R. Soc. Open Sci. 7. https://doi.org/10.1098/rsos.200065rsos200065.

Mittal, A.K., Kaler, A., Banerjee, U.C., 2012. Free radical scavenging and antioxidant activity of silver nanoparticles synthesized from flower extract of Rhododendron dauricum. Nano Biomed. Eng. 4, 118–124. https://doi.org/10.5101/nbe.v4i3.p118-124.

Mohammadinejad, R., Shavandi, A., Raie, D.S., Sangeetha, J., Soleimani, M., Shokrian Hajibehzad, S., Thangadurai, D., Hospet, R., Popoola, J.O., Arzani, A., Gómez-Lim, M.A., Iravani, S., Varma, R.S., 2019. Plant molecular farming: production of metallic nanoparticles and therapeutic proteins using green factories. Green Chem. 21, 1845–1865. https://doi.org/10.1039/C9GC00335E.

Mohanta, Y.K., Panda, S.K., Jayabalan, R., Sharma, N., Bastia, A.K., Mohanta, T.K., 2017. Antimicrobial, antioxidant and cytotoxic activity of silver nanoparticles synthesized by leaf extract of Erythrina suberosa (Roxb). Front. Mol. Biosci. 4, 1–9. https://doi.org/10.3389/fmolb.2017.00014.

Mulroy, T.W., 1979. Spectral properties of heavily glaucous and non-glaucous leaves of a succulent rosette-plant. Oecologia 38, 349–357. https://doi.org/10.1007/BF00345193.

Murad, U., Barkatullah, Khan, S.A., Ibrar, M., Ullah, S., Khattak, U., 2018. Synthesis of silver and gold nanoparticles from leaf of Litchi chinensis and its biological activities. Asian Pac. J. Trop. Biomed. 8, 142–149. https://doi.org/10.4103/2221-1691.227995

Nadagouda, M.N., Iyanna, N., Lalley, J., Han, C., Dionysiou, D.D., Varma, R.S., 2014. Synthesis of silver and gold nanoparticles using antioxidants from blackberry, blueberry, pomegranate, and turmeric extracts. ACS Sustain. Chem. Eng. 2, 1717–1723. https://doi.org/10.1021/sc500237k.

Nath, D., Banerjee, P., 2013. Green nanotechnology - a new hope for medical biology. Environ. Toxicol. Pharmacol. 36, 997–1014. https://doi.org/10.1016/J.ETAP.2013.09.002.

Park, M.V.D.Z., Neigh, A.M., Vermeulen, J.P., de la Fonteyne, L.J.J., Verharen, H.W., Briedé, J.J., van Loveren, H., de Jong, W.H., 2011. The effect of particle size on the cytotoxicity, inflammation, developmental toxicity and genotoxicity of silver nanoparticles. Biomaterials 32, 9810–9817. https://doi.org/10.1016/J.BIOMATERIALS.2011.08.085.

Patil, M.P., Kim, G.D., 2017. Eco-friendly approach for nanoparticles synthesis and mechanism behind antibacterial activity of silver and anticancer activity of gold nanoparticles. Appl. Microbiol. Biotechnol. 101, 79–92. https://doi.org/10.1007/S00253-016-8012-8.

Raju, D., Vishwakarma, R.K., Khan, B.M., Mehta, U.J., Ahmad, A., 2014. Biological synthesis of cationic gold nanoparticles and binding of plasmid DNA. Mater. Lett. 129, 159–161. https://doi.org/10.1016/J.MATLET.2014.05.021.

Rauf, A., Ahmad, T., Khan, A., Maryam, Uddin, G., Ahmad, B., Mabkhot, Y.N., Bawazeer, S., Riaz, N., Malikovna, B.K., Almarhoon, Z.M., Al-Harrasi, A., 2021. Green synthesis and biomedicinal applications of silver and gold nanoparticles functionalized with methanolic extract of Mentha longifolia. Artif. Cells, Nanomedicine Biotechnol. 49, 194–203. https://doi.org/10.1080/21691401.2021.1890099

Rónavári, A., Igaz, N., Gopisetty, M.K., Szerencsés, B., Kovács, D., Papp, C., Vágvölgyi, C., Boros, I.M., Kónya, Z., Kiricsi, M., Pfeiffer, I., 2018. Biosynthesized silver and gold nanoparticles are potent antimycotics against opportunistic pathogenic yeasts and dermatophytes. Int. J. Nanomed. 13, 695–703. https://doi.org/10.2147/IJN.S152010.

Rónavári, A., Igaz, N., Adamecz, D.I., Szerencsés, B., Molnar, C., Kónya, Z., Pfeiffer, I., Kiricsi, M., 2021. Green silver and gold nanoparticles: biological synthesis approaches and potentials for biomedical applications. Molecules 26, 1–39. https://doi.org/10.3390/molecules26040844.

Saif, S., Tahir, A., Chen, Y., 2016. Green Synthesis of Iron Nanoparticles and Their Environmental Applications and Implications. Nanomater. 2016, Vol. 6, Page 209 6, 209. https://doi.org/10.3390/NANO6110209.

Scimeca, M., Bischetti, S., Lamsira, H.K., Bonfiglio, R., Bonanno, E., 2018. Energy Dispersive X-ray (EDX) microanalysis: a powerful tool in biomedical research and diagnosis. Eur. J. Histochem. 62, 89–99. https://doi.org/10.4081/EJH.2018.2841.

Suganthy, N., Sri Ramkumar, V., Pugazhendhi, A., Benelli, G., Archunan, G., 2018. Biogenic synthesis of gold nanoparticles from Terminalia arjuna bark extract: assessment of safety aspects and neuroprotective potential via antioxidant, anticholinesterase, and antiamyloidogenic effects. Environ. Sci. Pollut. Res. 25, 10418–10433. https://doi.org/10.1007/S11356-017-9789-4/FIGURES/8.

Tamuly, C., Hazarika, M., Borah, S.C., Das, M.R., Boruah, M.P., 2013. In situ biosynthesis of Ag, Au and bimetallic nanoparticles using Piper pedicellatum C.DC: green chemistry approach. Colloids Surf. B Biointerfaces 102, 627–634. https://doi.org/10.1016/j.colsurfb.2012.09.007.

Tehri, N., Vashishth, A., Gahlaut, A., Hooda, V., 2022. Biosynthesis, antimicrobial spectra and applications of silver nanoparticles:

current progress and future prospects. Inorg. Nano-Metal Chem. 52, 1–19. https://doi.org/10.1080/24701556.2020.1862212.

Tippayawat, P., Phromviyo, N., Boueroy, P., Chompoosor, A., 2016. Green synthesis of silver nanoparticles in aloe vera plant extract prepared by a hydrothermal method and their synergistic antibacterial activity. PeerJ 2016, 1–15. https://doi.org/10.7717/peerj.2589.

Venugopal, K., Rather, H.A., Rajagopal, K., Shanthi, M.P., Sheriff, K., Illiyas, M., Rather, R.A., Manikandan, E., Uvarajan, S., Bhaskar, M., Maaza, M., 2017. Synthesis of silver nanoparticles (Ag NPs) for anticancer activities (MCF 7 breast and A549 lung cell lines) of the crude extract of Syzygium aromaticum. J. Photochem. Photobiol. B Biol. 167, 282–289. https://doi.org/10.1016/J.JPHOTOBIOL.2016.12.013.

Vijilvani, C., Bindhu, M.R., Frincy, F.C., AlSalhi, M.S., Sabitha, S., Saravanakumar, K., Devanesan, S., Umadevi, M., Aljaafreh, M.J., Atif, M., 2020. Antimicrobial and catalytic activities of biosynthesized gold, silver and palladium nanoparticles from Solanum nigurum leaves. J. Photochem. Photobiol. B Biol. 202,. https://doi.org/10.1016/j.jphotobiol.2019.111713 111713.

Wang, C., Mathiyalagan, R., Kim, Y.J., Castro-Aceituno, V., Singh, P., Ahn, S., Wang, D., Yang, D.C., 2016. Rapid green synthesis of silver and gold nanoparticles using Dendropanax morbifera leaf extract and their anticancer activities. Int. J. Nanomed. 11, 3691–3701. https://doi.org/10.2147/IJN.S97181.

Wang, S., Qian, K., Bi, X., Huang, W., 2009. Influence of speciation of aqueous HAuCl4 on the synthesis, structure, and property of Au colloids. J. Phys. Chem. C 113, 6505–6510. https://doi.org/10.1021/JP811296M/SUPPL_FILE/JP811296M_SI_001.PDF.

Watanabe, K., Menzel, D., Nilius, N., Freund, H.J., 2006. Photochemistry on metal nanoparticles. Chem. Rev. 106, 4301–4320. https://doi.org/10.1021/CR050167G.

Wei, L., Lu, J., Xu, H., Patel, A., Chen, Z.S., Chen, G., 2015. Silver nanoparticles: synthesis, properties, and therapeutic applications. Drug Discov. Today 20, 595–601. https://doi.org/10.1016/J.DRUDIS.2014.11.014.

Xin Lee, K., Shameli, K., Miyake, M., Kuwano, N., Bt Ahmad Khairudin, N.B., Bt Mohamad, S.E., Yew, Y.P., 2016. Green Synthesis of Gold Nanoparticles Using Aqueous Extract of Garcinia mangostana Fruit Peels. J. Nanomater. 2016. https://doi.org/10.1155/2016/8489094

Zayed, M.F., Eisa, W.H., El-kousy, S.M., Mleha, W.K., Kamal, N., 2019. Ficus retusa-stabilized gold and silver nanoparticles: Controlled synthesis, spectroscopic characterization, and sensing properties. Spectrochim. Acta - Part A Mol. Biomol. Spectrosc. 214, 496–512. https://doi.org/10.1016/j.saa.2019.02.042.

Zhang, X.F., Shen, W., Gurunathan, S., 2016. Silver nanoparticle-mediated cellular responses in various cell lines: an in vitro model. Int. J. Mol. Sci. 17, 1603. https://doi.org/10.3390/ijms17101603.